Am J Physiol Gastrointest Liver Physiol
279: G757–G766, 2000.

Rotavirus alters paracellular permeability and energy metabolism in Caco-2 cells

KATHLEEN G. DICKMAN,[1,3] SCOTT J. HEMPSON,[1] JOSEPH ANDERSON,[3] SCOTT LIPPE,[2] LIMING ZHAO,[2] ROBERT BURAKOFF,[2,3] AND ROBERT D. SHAW[1,3]
[1]*Research Service, Department of Veterans Affairs Medical Center, Northport, 11768;*
[2]*Department of Medicine, Winthrop University Hospital, Mineola 11501; and*
[3]*Department of Medicine, University at Stony Brook, Stony Brook, New York 11733*

Received 11 January 1999; accepted in final form 12 May 2000

Dickman, Kathleen G., Scott J. Hempson, Joseph Anderson, Scott Lippe, Liming Zhao, Robert Burakoff, and Robert D. Shaw. Rotavirus alters paracellular permeability and energy metabolism in Caco-2 cells. *Am J Physiol Gastrointest Liver Physiol* 279: G757–G766, 2000.—Rotaviruses infect epithelial cells of the small intestine, but the pathophysiology of the resulting severe diarrhea is incompletely understood. Histological damage to intestinal epithelium is not a consistent feature, and in vitro studies showed that intestinal cells did not undergo rapid death and lysis during viral replication. We show that rotavirus infection of Caco-2 cells caused disruption of tight junctions and loss of transepithelial resistance (TER) in the absence of cell death. TER declined from 300 to 22 $\Omega \cdot cm^2$ between 8 and 24 h after infection and was accompanied by increased transepithelial permeability to macromolecules of 478 and 4,000 Da. Distribution of tight junction proteins claudin-1, occludin, and ZO-1 was significantly altered during infection. Claudin-1 redistribution was notably apparent at the onset of the decline in TER. Infection was associated with increased production of lactate, decreased mitochondrial oxygen consumption, and reduced cellular ATP (60% of control at 24 h after infection), conditions known to reduce the integrity of epithelial tight junctions. In conclusion, these data show that rotavirus infection of Caco-2 intestinal cells altered tight junction structure and function, which may be a response to metabolic dysfunction.

oxygen consumption; lactate; ATP; transepithelial resistance; zonula occludens; tight junctions; claudin-1; occludin

ROTAVIRUS IS THE MAJOR ETIOLOGIC agent of severe diarrhea in infants and young children. The pathophysiology of gastroenteritis remains incompletely understood. Rotaviruses replicate in the differentiated columnar epithelial cells of the intestinal villi, and infection is associated with blunting of the villi and infiltration of the lamina propria by mononuclear cells (19). The magnitude of the pathological changes appears to be variable, and it is uncertain whether a direct link exists between tissue damage and diarrhea. For example, simian rotavirus infection of mice produces diarrhea, although pathological changes are limited to moderate swelling and vacuolation of epithelial cells (32).

Recent studies indicate that dysregulation of the paracellular pathway may be important in the pathogenesis of diarrheal disease. *Vibrio cholera*-derived zonula occludens toxin can promote diarrhea by impairing the integrity of epithelial tight junctions (11). *Salmonella*, *Escherichia coli*, and *Bacteroides fragilis* specifically alter tight junction permeability, perhaps by engagement of the actin cytoskeleton (4, 6, 12, 31, 40). Recent Ussing chamber studies of HIV-infected human intestine from subjects with diarrhea demonstrated reduced transepithelial resistance (TER) and barrier function that could, the authors proposed, contribute to diarrhea by passive leak mechanisms (41).

The well-documented infection of Caco-2 cells by rotavirus has become the most widely studied in vitro model of rotavirus infection of intestinal cells (17, 21, 42). Caco-2 cells are an extensively characterized model system for intestinal epithelial permeability (14). Cells develop polarization of distinct apical and basolateral surfaces separated by tight junctions at areas of cell-to-cell contact. Monolayers grown on collagen-coated filters develop a TER of 300–600 $\Omega \cdot cm^2$ and are relatively impermeable to molecules of molecular masses of 400–70,000 Da. Three recent reports have evaluated Caco-2 intestinal epithelial cells grown on collagen-coated filter supports as a model of rotavirus interactions with host cells (17, 18, 42). These studies showed that rotavirus infection of Caco-2 cells caused a loss of TER in the absence of cell death, leading to speculation that infection may alter paracellular permeability.

In this series of experiments, we demonstrated that rotavirus infection of Caco-2 intestinal cells caused increased paracellular permeability that was associated with metabolic dysfunction. This demonstration of a novel cellular response to rotavirus infection has important implications for diarrhea pathogenesis in viral gastroenteritis.

Address for reprint requests and other correspondence: R. D. Shaw, Research Service, Bldg. 62 (151), Northport Veterans Affairs Medical Center, Northport, NY 11768 (E-mail: rds@who.net).

The costs of publication of this article were defrayed in part by the payment of page charges. The article must therefore be hereby marked "*advertisement*" in accordance with 18 U.S.C. Section 1734 solely to indicate this fact.

MATERIALS AND METHODS

Cell lines. Caco-2 cells were obtained from the American Type Culture Collection. Cells were passed weekly and maintained in a 1:1 mixture of DMEM [nutrient mixture F-12 (DMEM-F12) supplemented with 15 mM HEPES, 2 mM glutamine, 15 mM sodium bicarbonate, 100 U/ml penicillin, 100 μg/ml streptomycin, and 10% fetal calf serum]. Cultures were maintained in a 37°C incubator with 5% CO_2. All experiments were performed with cultures 3–5 days after confluency. Pilot experiments with monolayers aged to 21 days postconfluence demonstrated no differences in rotavirus infectivity or loss of TER. Therefore, 3–5 days after confluence was used for the experiments reported in this study.

Virus preparation and infection. Rhesus rotavirus (RRV) was cultivated in and isolated from MA104 cell cultures as previously described (45). Virus was collected from culture medium by fluorocarbon extraction and sucrose gradient centrifugation. Virus bands were identified by hemagglutination assays, followed by dialysis against Tris-saline-2 mM $CaCl_2$ and concentration by ultracentrifugation. Virus titers were determined by standard hemagglutination and immunohistochemical focus assays (39). To infect Caco-2 cultures, monolayers were washed twice in serum-free medium and then exposed to virus [multiplicity of infection (moi) = 10] in serum-free DMEM-F12. RRV was activated with trypsin (2.5 μg/ml for 30 min at 37°C) before use. Sham-infected monolayers treated with identical medium absent virus were used as the noninfected controls.

TER. Caco-2 cells were grown as confluent monolayers on collagen-coated cell culture inserts (6.4-mm diameter Biocoat inserts, Collaborative Research). One week after plating, the inserts were transferred from 24-well dishes into 6-well dishes, rinsed with PBS, and incubated 16 h in serum-free DMEM-F12 (0.3 ml apical and 9 ml basolateral volumes) before virus exposure. Overnight incubation ensured temperature and pH equilibration and prevented transient electrical fluctuations that occur after media changes and repetitive measurements. TER was measured with an epithelial volt-ohmmeter (WPI, Sarasota, FL). Values were corrected for background resistance (150 Ω) and normalized to surface area (0.3 cm^2). Resistance was measured just before virus addition and at various times thereafter up to 24 h. Trypsin-activated RRV (moi = 10) was added to the apical solution.

Permeability measurements. We determined the permeability of Caco-2 monolayers by measuring transepithelial passage of three probes of graded mass as previously described (38). These probes included fluorescein sulfonic acid (FS, 478 Da; Molecular Probes) and fluorescein-isothiocyanate dextran of molecular masses of 4 kDa and 70 kDa (FD4 and FD70; Sigma). Caco-2 monolayers on collagen-coated inserts were infected as described above with RRV (moi = 10) and incubated at 37°C in 5% CO_2 for 20 h. Monolayers consistently showed >70% loss of TER at this time (Fig. 1). FS (final concentration, 200 μg/ml), FD4 (25 mg/ml), or FD70 (20 mg/ml) was added to the basolateral chamber, and the cultures were placed on a rotary shaker in a 5% CO_2 incubator at 37°C to ensure adequate mixing. Samples (4 μl) of the apical and basolateral chambers were diluted in 1 ml of water and analyzed for fluorescence using a Perkin Elmer LS-5 fluorescence spectrophotometer at an excitation wavelength of 492 nm and an emission wavelength of 515 nm. The permeability of the monolayers was expressed as clearance, calculated as the basolateral-to-apical flux of the probe divided by the concentration of the probe in the basal compartment, as previously described (29). The clearance measurements were reported for a 2-h period beginning 1 h after probe addition, or 21–23 h postinfection (hpi). Clearance between 23 and 24 hpi was also measured to document linearity throughout the experimental period. The permeability of noninfected monolayers was minimal and consistent. However, matched uninfected controls were included with each experiment.

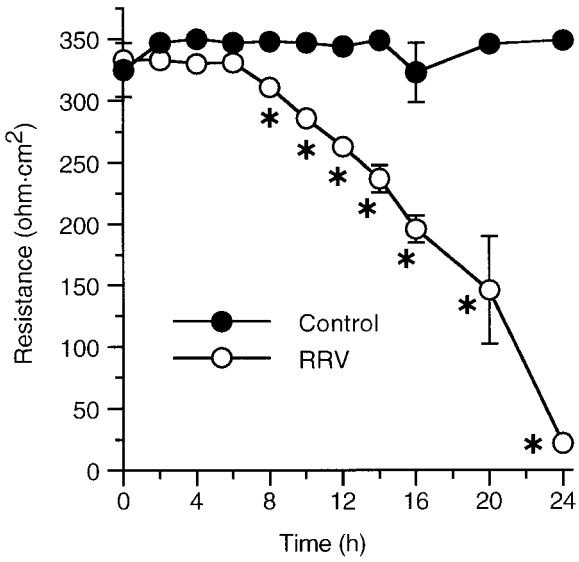

Fig. 1. Transepithelial resistance (TER) of Rhesus rotavirus (RRV)-infected Caco-2 monolayers. Time course for the decline in TER observed after infection of Caco-2 cells with RRV [multiplicity of infection (moi) = 10]. Values are means ± SE; $n = 4$. *$P < 0.05$ vs. control.

Microscopy. The tight junction proteins claudin-1, occludin, and zonula occludens-1 (ZO-1) were similarly detected in rotavirus- (and sham-) infected Caco-2 monolayers. At the indicated times after infection, cells were fixed with methanol (−80°C) and incubated for 1 h with a 1:100 dilution of rabbit anti-claudin-1, anti-occludin, or anti-ZO-1 antibodies (Zymed), followed by anti-rabbit monoclonal antibody conjugated to fluorescein at 1:100 dilution for 1 h (Sigma). Results were analyzed with epifluorescent or laser scanning confocal microscopy. Digital images were processed identically with Metamorph software.

Cell viability. Cell viability was assessed with the 3-(4,5-dimethylthiazol-2-yl)-2,5-diphenyl tetrazolium bromide (MTT) assay for mitochondrial dehydrogenase activity (Sigma). Cultures were treated with 0.5 mg/ml MTT for 3 h, and the reaction was stopped by addition of an equal volume of acidic isopropanol. Samples were briefly sonicated to ensure dissolution of the colored product, and absorbance was read on a spectrophotometer at 570 λ with background correction at 690 λ.

Oxygen consumption. Mitochondrial respiration was assessed with oxygen consumption (Q_{O_2}) measurements using cells after various times of infection with RRV. Medium was aspirated from 60-mm dish cultures, and the cells were gently scraped with a rubber policeman into 2.5 ml of fresh serum-free DMEM-F12. Cell suspensions were gassed with 95% air-5% CO_2 and incubated in a rotary water bath at 37°C for 7 min. Suspensions were transferred into a sealed 37°C chamber equipped with a Clarke-type oxygen electrode. Oxygen tension was monitored with a Yellow Springs oxymeter and recorded as a function of time with a Zip-Konnen chart recorder. After a stable basal rate of Q_{O_2} was achieved, ATP utilization by the Na^+-K^+-ATPase was assessed by measur-

ing Qo_2 after addition of ouabain (final concentration 1 mM) to the chamber. Basal Qo_2 was calculated as the sum of ouabain-sensitive and -insensitive Qo_2. Qo_2 rates were normalized to cell protein as previously described (9). Protein was measured with the Bradford assay using BSA as a standard.

Lactate and ATP measurements. Caco-2 cells were grown in 35-mm dishes for lactate and ATP measurements. Medium lactate concentration was measured by spectrophotometric assay (Sigma). Cellular ATP content was assayed by the luciferin/luciferase method on a Turner Designs 20/20 luminometer using reagents available from Turner. ATP was extracted from the cultures by incubation in lysis buffer (1 ml/35 mm dish) for 20 min. Extracts (5–10 μl) were added to 900 μl of reaction buffer, and light emission was measured for 15 s after a preset 3-s delay. ATP content was normalized to cellular protein as described above.

Statistics. Data are presented as means ± SE. Statistical significance was determined by unpaired *t*-test. Comparisons with a P value <0.05 were considered statistically significant.

RESULTS

TER. TER of untreated Caco-2 monolayers averaged 325 ± 22 $\Omega \cdot cm^2$ and remained constant for 24 h (Fig. 1). In monolayers exposed to RRV, a slight but significant drop in resistance was first observed at 8 hpi. Resistance continued to decline over time and reached 22 ± 3 $\Omega \cdot cm^2$ by 24 h. The rate of decline was linear (r^2 = 0.99) between 8 and 20 h and averaged 14 $\Omega \cdot cm^2 \cdot h^{-1}$. We also tested whether virus binding and penetration was required for this response by pretreating RRV with EDTA to release the outer protein capsid. Viral particles lacking an outer capsid do not bind or penetrate cell membranes and had no effect on TER after 24 h exposure (350 ± 23 vs. 307 ± 12 $\Omega \cdot cm^2$, control vs. single-shell RRV; n = 3; not significant).

Myosin light-chain phosphorylation is an important mechanism by which some intestinal pathogens regulate tight junctions (36, 40, 53). Therefore, we repeated the experiments above in the presence of the myosin light-chain kinase inhibitor ML-9 (Calbiochem, La Jolla, CA). ML-9 (30 μM) was applied 1 h before RRV infection. ML-9 did not alter TER in control monolayers, nor did it prevent time of onset or rate of loss of TER during RRV infection (data not shown).

Cell viability. Because cell death or loss from the monolayer may lead to loss of TER, we examined cell viability after RRV infection. Monolayers remained intact at 24 hpi as observed by phase contrast microscopy (see Fig. 2). At 24 hpi, the MTT viability assay revealed no significant difference between control and infected monolayers (Fig. 3*A*), and the protein content per culture dish (Fig. 3*B*) was unaffected, indicating no loss of cells. Thus cytotoxicity from viral infection was not observed during these studies.

Domes are formed by Caco-2 monolayers grown on nonporous surfaces. These structures are thought to represent areas of net fluid absorption (24). Domes are present in untreated monolayers (Fig. 2*A*) but are diminished within 24 h after rotavirus infection (Fig. 2*B*). This may be expected if the tight junctions are disrupted by infection.

Permeability of Caco-2 monolayers. Because the loss of TER and domes suggested that RRV altered barrier function, we assessed the permeability of three fluorescent probes of graded molecular weights. Permeability of the Caco-2 monolayers to FS and FD4 was significantly increased during infection by RRV (Fig. 4). To determine the average clearance for each probe, 7–9 experimental monolayers and an equal number of mock-infected control monolayers were studied. The clearance of FS under control conditions was 446 ± 91 $nl \cdot h^{-1} \cdot cm^{-2}$. This increased to 16,910 ± 5,744 $nl \cdot h^{-1} \cdot cm^{-2}$ (38-fold increase) between 21 and 23 hpi (P = 0.02). Treatment of the monolayer with EDTA (5 mM added to apical side for 15 min) to completely open tight junctions increased the clearance to 64,768 ± 10,337 $nl \cdot h^{-1} \cdot cm^{-2}$. To provide a relative measure of the RRV-induced permeability, we calculated the ratio of RRV to EDTA, which was 26.1%. Permeability to FD4 was also increased significantly, because the clearance rose from 168 ± 36 to 5,733 ± 2,081 $nl \cdot h^{-1} \cdot cm^{-2}$ (a 34-fold increase; P = 0.014). After EDTA treatment, the FD4 clearance increased to 17,741 $nl \cdot h^{-1} \cdot cm^{-2}$ and the calculated RRV/EDTA ratio was 32.3%. FD70 permeability did appear to increase during RRV infection (from 55 to 399 $nl \cdot h^{-1} \cdot cm^{-2}$, a sevenfold increase), but the increase was not statistically significant (P = 0.1886) and the ratio of RRV to EDTA clearances was only 11%. Therefore, we concluded that the permeability induced by RRV was relatively size selective, permitting substantial flux of the 478- and 4,000-Da probes but only

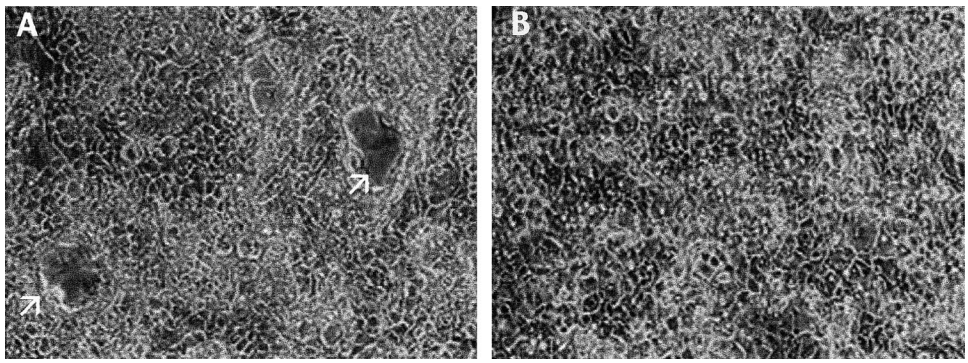

Fig. 2. Phase-contrast microscopy of infected monolayers. Caco-2 monolayers were grown to confluence, washed with serum-free medium, and then infected with RRV (moi = 10). *A*: mock-infected control monolayers incubated for 24 h. *B*: RRV-infected monolayers for the corresponding time. Low-power phase-contrast microscopy shows domes (arrows) in the control but not in the RRV-infected monolayer.

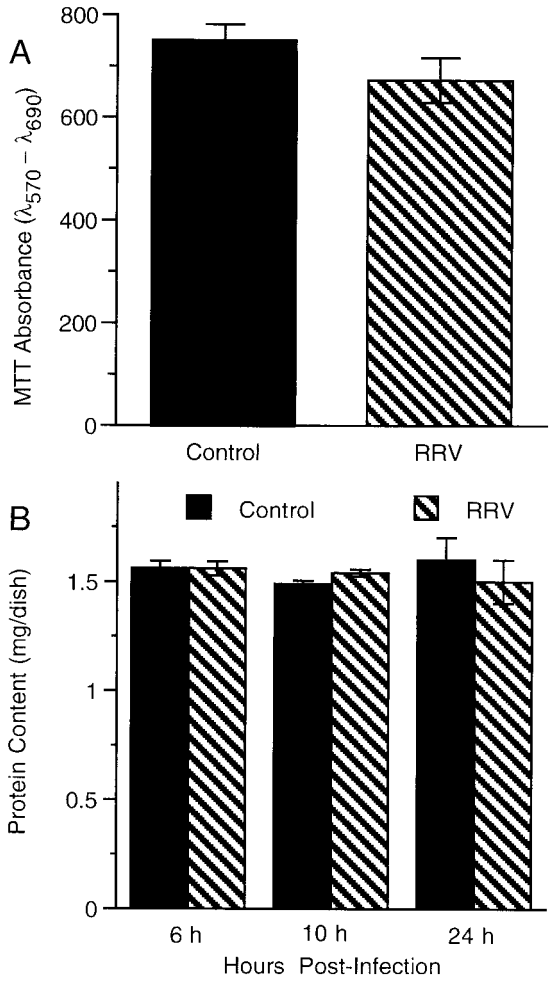

Fig. 3. *A*: 3-(4,5-dimethylthiazol-2-yl)-2,5-diphenyl tetrazolium bromide (MTT) viability assay. Caco-2 cell monolayers were mock- or RRV-infected as in Fig. 2 and incubated for 24 h. The MTT assay indicated no significant difference in cell viability at that time (n = 14). *B*: dish protein content. Protein from Caco-2 cells cultured on 35-mm dishes was measured as a function of time following RRV infection. No significant loss of cells was noted over a 24-h infection period (n = 3–5).

limited flux of the 70,000-Da probe. These findings indicate that RRV-induced permeability changes apply to both charged (FS) and uncharged (FD4) compounds.

Tight junction proteins. Because increased paracellular permeability may be accompanied by alterations in the subcellular distribution of tight junction proteins, we used immunohistochemistry to detect changes in the localization of three tight junction-specific proteins (49), claudin-1, occludin, and ZO-1, during RRV infection. As shown by epifluorescent microscopy (Fig. 5), significant changes in claudin-1 distribution were noted at 10 hpi, a time when TER was beginning to decline. In control cultures, claudin-1 immunostaining was present as a strong, continuous pericellular band. This pericellular staining pattern was diminished with viral infection at 10 hpi, coincident with the appearance of marked cytoplasmic foci.

Confocal microscopy was used to compare the distribution of occludin and claudin-1 in RRV-infected and sham-infected monolayers at various times after infection (Fig. 6). The initial patterns of both proteins showed nearly exclusive localization to the pericellular regions, as expected (Fig. 6, *A* and *D*). No changes were noted in sham-infected monolayers throughout the 18-h experimental period (data not shown). At 10 hpi there was a striking loss of pericellular claudin-1, and a marked cytoplasmic accumulation of the protein was readily visible throughout the monolayer (Fig. 5*B*). By 18 hpi, nearly complete movement of the stainable claudin-1 to cytoplasmic foci was observed (Fig. 6*C*). Occludin, on the other hand, remained mostly intact in the pericellular region at 10 hpi, with only a mild loss of signal detected in some regions of the monolayer (Fig. 6*E*). However, at 18 hpi pericellular occludin staining was markedly diminished (Fig. 6*F*).

In addition to occludin and claudin-1, we also used confocal microscopy to examine ZO-1, a protein that is believed to link these two integral membrane protein components of the tight junction to the actin cytoskeleton. ZO-1 was present as a distinct and continuous pericellular band in control cultures, as shown in Fig. 7. Two notable changes in ZO-1 immunostaining were observed with RRV infection by 18 hpi. First, the intensity of pericellular staining was markedly diminished (Fig. 7, *B* and *C*). Second, intercellular gaps in ZO-1 staining were frequently observed (Fig. 7*B*), perhaps as a consequence of altered cell shape.

Cellular energy metabolism. The consequences of rotavirus infection on cellular energy metabolism are

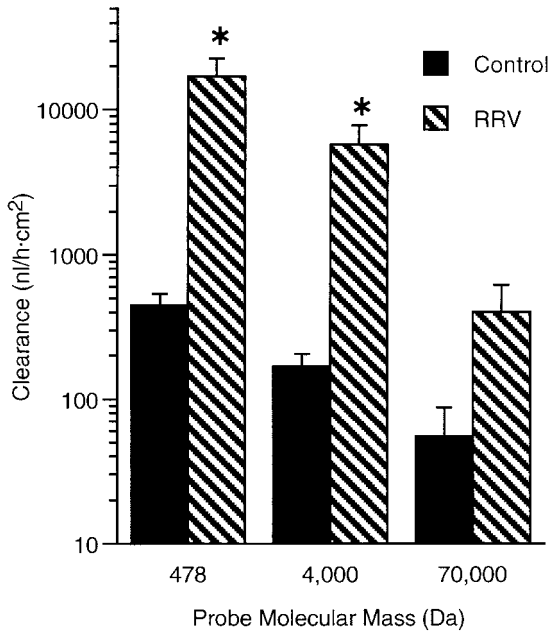

Fig. 4. Transepithelial permeability of Caco-2 monolayers during RRV infection. Confluent monolayers were infected with RRV (moi = 10) for 21 h, at which time resistance was decreased at least 70% from controls. Transepithelial passage (basolateral to apical) of fluorescent probes of graded molecular masses (478 Da fluorescein sulfonic acid, 200 μg/ml; 4,000 Da FITC-dextran, 25 mg/ml; and 70,000 Da FITC-dextran, 20 mg/ml) was measured from 21 to 23 h postinfection (hpi). Clearance of 478- and 4,000-Da probes was significantly increased (*$P < 0.05$) with RRV infection compared with controls (n = 7).

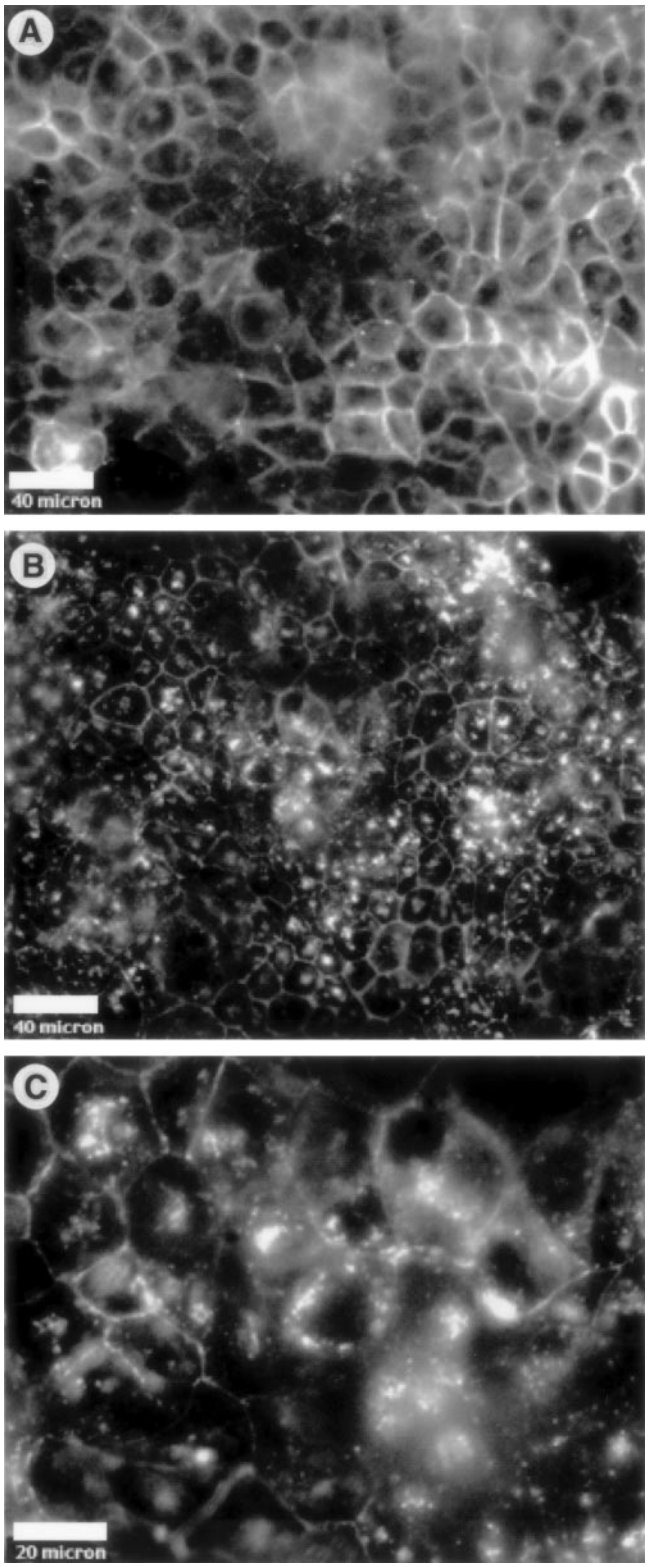

Fig. 5. Rotavirus infection alters distribution of claudin-1. Confluent monolayers of Caco-2 cells were mock- or RRV-infected (moi = 10), fixed, stained for the presence of claudin-1, and examined by epifluorescent microscopy. *A*: noninfected monolayer. *B* and *C*: similar monolayer 10 hpi. The pervasive nature of the abnormality can be clearly seen in *B*. *C* shows greater detail of the cytoplasmic aggregations.

unknown. However, in other studies of Caco-2 cells, lactic acidosis and ATP depletion caused increased tight junction permeability (29, 52). Because we observed that RRV infection caused increased medium acidification over time, we tested for altered lactate production. The pH in infected monolayer supernatants averaged 6.71 ± 0.04 at 24 hpi, compared with control monolayers at pH 6.94 ± 0.02 ($n = 7$; $P < 0.003$). As shown in Fig. 8, 16-h exposure to RRV significantly increased medium lactate levels in Caco-2 cultures. Time course studies were conducted to determine when the increase in lactate production occurred. During the first 4 hpi, RRV had no significant effect on lactate production. Between 4 and 8 hpi, the rate slightly increased with infection (5.6 ± 0.3 vs. 8.0 ± 0.6 $nmol \cdot min^{-1} \cdot mg^{-1}$ protein, control vs. RRV; $P < 0.05$), whereas at 8–12 hpi, the rate of lactate production was three times higher than control (4.9 ± 0.3 vs. 14.4 ± 0.5 $nmol \cdot min^{-1} \cdot mg^{-1}$ protein, control vs. RRV; $P < 0.05$).

Stimulation of glycolysis may be a compensatory response to inhibition of mitochondrial ATP production (8). Therefore, the effect of RRV on mitochondrial respiration was examined by Q_{O_2} measurements. Impaired mitochondrial activity in Caco-2 cells was evident at 10 hpi (Fig. 9). Basal respiration was inhibited with RRV treatment by 51%. Ouabain-sensitive Q_{O_2}, which represents the energy used to support Na^+-K^+-ATPase activity, was reduced by 68%. Ouabain-insensitive respiration, which represents ATP utilization by protein synthesis and other energy-consuming processes, was also inhibited with RRV infection (59% of control). Effects of RRV on respiration in Caco-2 cells were evident as early as 6 hpi (data not shown). Basal respiration was inhibited to a comparable degree at 6 and 10 hpi (3.9 ± 0.6 vs. 3.8 ± 0.4 $nmol \cdot min^{-1} \cdot mg^{-1}$, 6 vs. 10 h; not significant).

To determine the effect of altered lactate production and mitochondrial function on energy balance, we measured cellular ATP levels in Caco-2 cells at various times after infection (Fig. 10). No significant changes in ATP levels were seen at 6 and 10 hpi despite the marked reduction in mitochondrial respiration observed at these times. A drop in the ATP content of infected cells to 40% of control monolayers was noted at 24 hpi.

DISCUSSION

A critical function of the small intestinal epithelium is to maintain a highly selective barrier between the lumen and the systemic circulation. Microorganisms and macromolecules must be excluded, and the flow of water and solutes must be regulated. The integrity of the epithelial barrier depends on the maintenance of the selective permeability properties of the tight junctions. Paracellular permeability is altered in response to bacterial pathogens such as *Clostridium difficile*, enterohemorrhagic *E. coli* (36), enteropathogenic *E. coli* (40), and the cholera zonula occludens toxin (11), as well as the toxin okadaic acid that is associated with diarrheic shellfish poisoning (46). Paracellular perme-

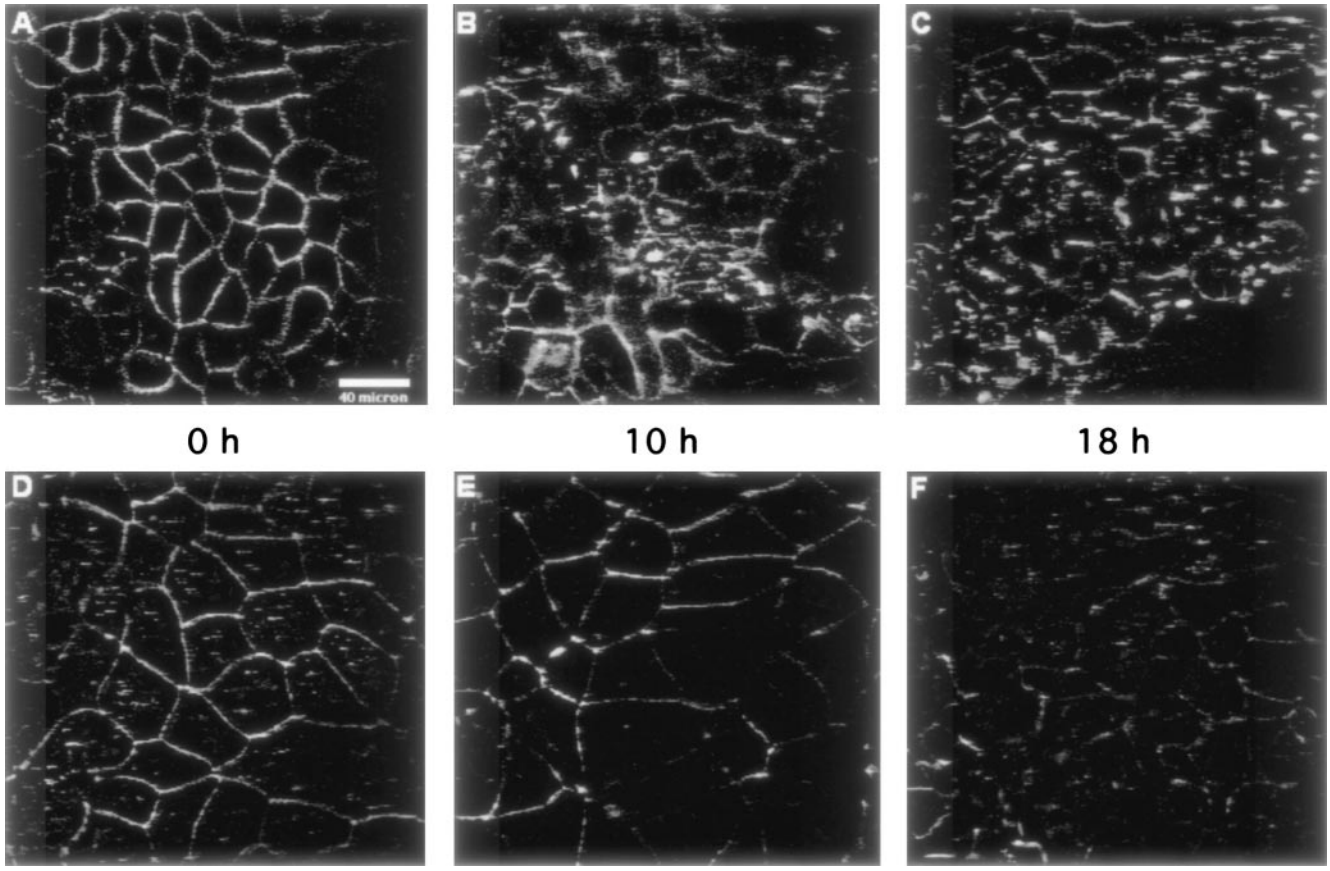

Fig. 6. Rotavirus infection disrupts the distribution of the tight junction proteins claudin-1 and occludin at 10 and 18 hpi. Confluent monolayers were infected with RRV as in Fig. 5. Cells were fixed and stained at the designated times for either claudin-1 (*A–C*) or occludin (*D–F*). All images were obtained from confocal microscopy and are of the same magnification and identically processed. Bar, 40 μm.

ability contributes significantly to diarrhea in these diseases. Recently, endoscopic biopsies from HIV-infected patients suffering from diarrhea in the absence of enteric pathogens were studied in customized Ussing chambers (41). Neither ion secretion nor impaired absorption of sodium or glucose was found, but reduced barrier function was strongly associated with diarrhea (a 40% reduction in TER compared with HIV-infected nondiarrheic controls).

Paracellular permeability changes may contribute to disease by altering intestinal secretion and absorption and by permitting penetration of the mucosa by potentially toxic or inflammatory substances. Hyperpermeability of the intestine during rotavirus infection has

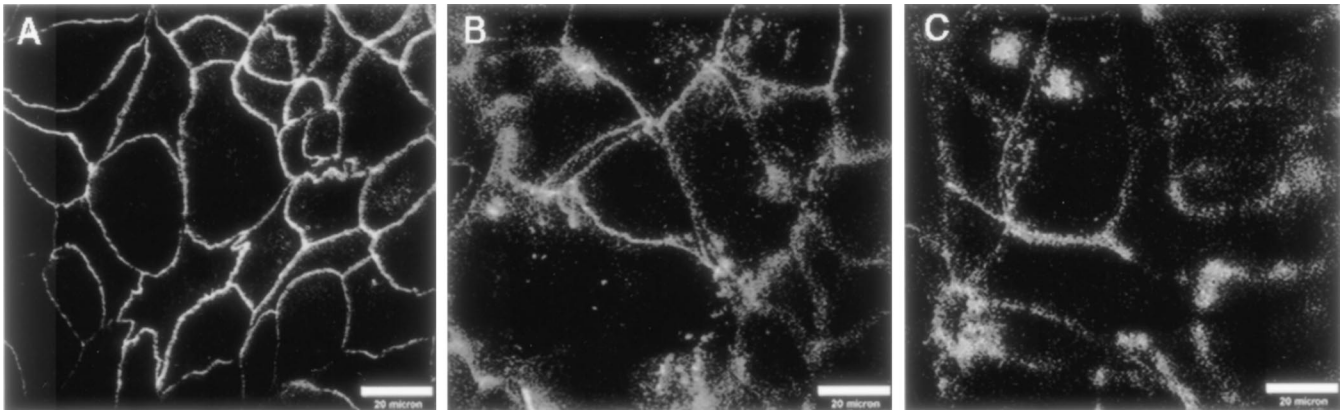

Fig. 7. Rotavirus infection disrupts the distribution of the tight junction protein ZO-1. Caco-2 cell monolayers were prepared and infected with RRV as in Fig. 5. *A*: distribution of ZO-1 before infection. *B* and *C*: ZO-1 at 18 hpi. In regions in which pericellular staining is somewhat preserved, gaps frequently appear between the ZO-1 bands of adjacent cells (*B*). Bars, 20 μm.

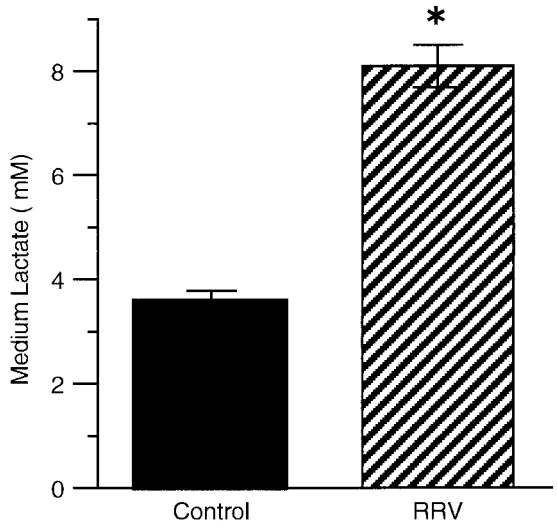

Fig. 8. Lactate production rate during RRV infection of Caco-2 cells. Confluent monolayers of Caco-2 cells were mock- or RRV-infected (moi = 10). Culture supernatants were assayed for lactate concentration at 16 hpi. Medium lactate concentration was significantly increased with RRV infection (*$P < 0.01$; $n = 11$).

been documented in vivo with enteral markers such as lactulose and mannitol (15, 16, 50). We are not aware of studies that evaluated blood-to-lumen clearance during infection, although presumably loss of tight junction integrity results in a reciprocal loss of barrier function.

In this study, we showed that rotavirus infection of Caco-2 monolayers increased transepithelial macromolecular paracellular permeability. We also showed that rotavirus infection alters the distribution of two transmembrane components of epithelial tight junctions, claudin-1 and occludin, as well as the membrane-asso-

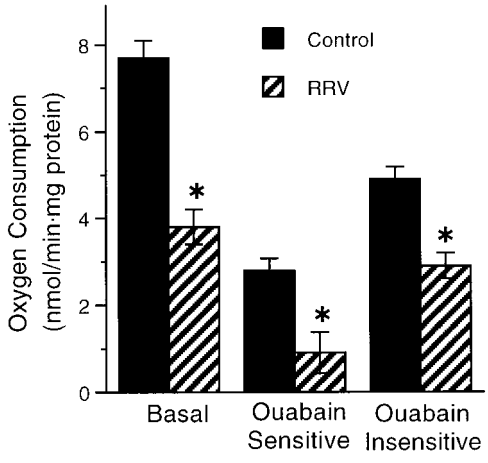

Fig. 9. Mitochondrial oxygen consumption rates (Q_{O_2}) during RRV infection of Caco-2 cells. Confluent monolayers of Caco-2 cells were mock- or RRV-infected (moi = 10), and Q_{O_2} was measured at 10 hpi as described in MATERIALS AND METHODS. After a stable basal rate of Q_{O_2} was achieved, ATP utilization by the Na^+-K^+-ATPase was assessed by measuring Q_{O_2} after addition of ouabain (final concentration 1 mM) to the chamber. The sum of ouabain-sensitive and -insensitive Q_{O_2} is equal to the basal Q_{O_2}. RRV infection caused a significant decrease in basal, ouabain-sensitive, and ouabain-insensitive Q_{O_2} at 10 hpi (*$P < 0.05$; $n = 3$–8).

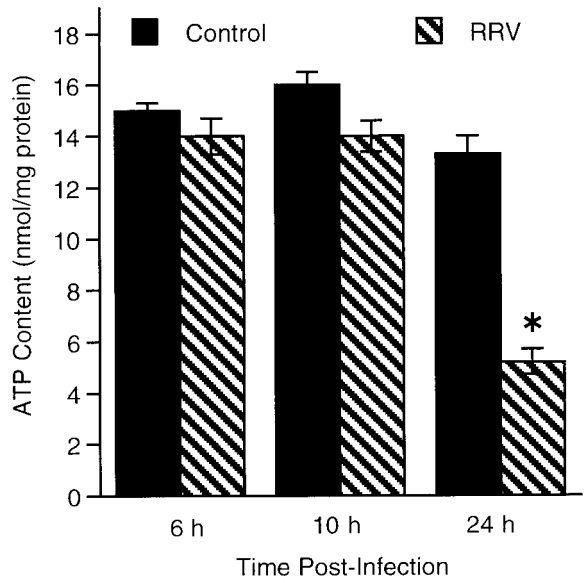

Fig. 10. ATP levels as a function of time during RRV infection of Caco-2 cells. Confluent monolayers of Caco-2 cells were mock- or RRV-infected (moi = 10). Cellular ATP content (normalized to protein) was measured at 6, 10, and 24 hpi. A significant decrease in ATP content was noted with RRV infection at 24 hpi (*$P < 0.05$; $n = 3$–8).

ciated cytoplasmic protein ZO-1 that serves to link occludin and the actin cytoskeleton (10). These structural alterations in the tight junctions occur contemporaneously with changes in TER and paracellular permeability.

Occludin is an integral membrane protein that is one of the major constituents of tight junction strands (structure reviewed in Ref. 49). Claudin-1 is a distinct transmembrane protein that is a member of a new gene family including at least 15 members. Claudins and occludin copolymerize to form the backbone of tight junction strands. ZO-1 is a member of the protein family known as membrane-associated guanylate kinase homologues, which localize to the cytoplasmic side of tight junctions. ZO-1 binds to occludin at its amino terminal half and to actin filaments at the carboxy terminus, thereby forming a bridge between the tight junction strands and the actin cytoskeleton. Thus during rotavirus infection we identified abnormal distribution of the major components of both tight junction strands and cytoplasmic scaffolding.

Several studies using epithelial cell lines identified ATP depletion as a cause of paracellular hyperpermeability and redistribution of tight junction proteins (20, 26, 38, 52). ATP depletion was previously associated with changes in the actin cytoskeleton, notably a diminution and disruption of F-actin in areas of cell-to-cell contact after chemical hypoxia was initiated in Caco-2 cells (1, 48, 52). Recently, Brunet et al. (3) showed that RRV infection in Caco-2 cells caused F-actin reorganization beginning at 18 hpi, particularly in the microvillus regions. We have performed actin studies and obtained very similar results (data not shown). They also presented evidence that the actin reorganization is mediated by increased intracellular calcium concentra-

tion. Reorganization of the actin cytoskeleton may alter tight junction function because actin filaments are linked to tight junction proteins. However, there is as yet no evidence that the decline in TER or tight junction reorganization is mediated by changes in the actin filaments or intracellular calcium concentration.

In addition to effects on actin, ATP depletion was reported to alter the distribution of tight junction proteins in epithelial cells (30, 47). These changes included loss of pericellular localization and increased cytoplasmic aggregation of occludin and ZO-1 (48), similar to the changes we observed during RRV infection. Also, separation of cellular boundaries in the ZO-1 images (Fig. 7) from infected cells is similar to the paracellular "gaps" depicted by Tsukamoto and Nigam (48) during ATP depletion in epithelial cells. There are as yet no studies to link ATP depletion to reorganization of the recently described claudin-1 protein.

Enhanced glucose entry into cells may be a common response of cells during the early stages of viral infection. Sindbis virus (13), cytomegalovirus (22), vesicular stomatitis virus (35), and Semliki forest virus (34, 43) have all been shown to increase hexose entry into infected cells. In the case of Semliki forest virus, it was shown that hexose entry is facilitated during viral infection via translocation of glucose transporters to the plasma membrane. It is believed that some glucose entering cells during viral infection is converted into lactate, consistent with our findings that lactate production was stimulated with RRV infection in Caco-2 cells. The increased glycolytic activity seen during RRV infection may also provide an alternative energy source when oxidative phosphorylation is compromised by the observed inhibition of mitochondrial respiratory activity.

Little is known of the effects of viral infection on mitochondrial function. Infection of glia and renal epithelial cells with feline immunodeficiency virus has been shown to decrease mitochondrial membrane potential (7), which typically indicates impaired mitochondrial function. Others have shown that mitochondria cluster within the cell in areas of viral assembly (37), suggesting that cellular ATP may be diverted to support the energy demands of virus replication. In the case of RRV-infected Caco-2 cells, we noted that cellular Qo_2 was inhibited by 50% within 6–10 h. A negative feedback response to the increased lactate production we observed is one possible explanation for this inhibition. There is normally a balance between ATP production and consumption within cells providing constant ATP content. If ATP generation from lactate production is increased via enhanced glucose entry into the cell, the mitochondria should respond by proportionately decreasing ATP production by oxidative phosphorylation. Alternatively, there may be some aspect of viral infection that directly compromises mitochondrial function. Possible candidates include interferon-α or -β. These cytokines may be induced with viral infection and have been shown to reduce mitochondrial levels of cytochrome *b*, cytochrome oxidase, and NADH cytochrome *c* reductase, leading to ATP depletion (23).

Assuming that one ATP molecule is generated per molecule of lactate produced, the average glycolytic ATP production rate increased during RRV infection by 10 $nmol \cdot min^{-1} \cdot mg^{-1}$ compared with control rates at 8–12 hpi. Assuming 6 ATP molecules are produced per molecule of oxygen consumed, mitochondrial ATP production was inhibited by 24 $nmol \cdot min^{-1} \cdot mg^{-1}$ compared with control at 10 hpi. Thus the increased ATP produced by glycolysis did not fully offset the reduction in ATP production by the mitochondria, which should lead to ATP depletion. However, ATP levels remained unchanged at 6 and 10 hpi despite this imbalance, suggesting a decrease in ATP utilization, although ATP depletion did occur sometime between 10 and 24 hpi, coincident with the drop in TER.

The discovery of numerous cytokine receptors on intestinal epithelial cells has promoted consideration of epithelial dysfunction in inflammatory diarrheal diseases (33, 44). Tumor necrosis factor (TNF) in particular alters paracellular permeability of Caco-2 monolayers to sodium and chloride but not mannitol (27). Rotavirus is known to stimulate epithelial cells to secrete cytokines (5, 39). However, these studies in rotavirus-infected intestinal epithelial cell cultures and murine intestine did not detect induction of TNF-α mRNA nor TNF-α production. Other cytokines, such as interferon-γ derived from activated immune cells, have been shown to alter absorption, secretion, and barrier function of intestinal epithelial monolayers (25, 28). However, rotavirus diarrhea is unchanged in T cell-deficient Rag-2 mice that have markedly decreased levels of interferon-γ (R. Shaw, unpublished data). No evidence has yet been presented to demonstrate the role of cytokines or other immune activities in the generation of diarrhea during rotavirus infection, and cytokines of nonepithelial origin obviously are not involved in studies of pure Caco-2 cells.

The viral nonstructural protein NSP4 has been implicated as a causative agent for rotavirus disease. Diarrhea occurs when NSP4 is administered to young mice, and although not itself a secretagogue, NSP4 augments forskolin-stimulated chloride secretion in the intestine (2). NSP4 also increases intracellular calcium when expressed within insect cells (45) or when applied extracellularly to intestinal HT-29 cells (9). However, the importance of calcium-activated chloride secretion in rotavirus diarrhea has not been established. A plausible hypothesis to test in future studies concerns the effects of NSP4 on paracellular permeability, since intracellular calcium has been shown to play a key role in the maintenance of tight junction integrity (51). Alternatively, intracellular calcium may be elevated because of ATP depletion during RRV infection and may be responsible for permeability changes. Thus rotavirus effects on calcium homeostasis may cause diarrhea by more than one mechanism either simultaneously or during sequential stages of the illness.

This work was supported by Department of Veterans Affairs Medical Research funds.

REFERENCES

1. **Bacallao R, Garfinkel A, Monke S, Zampighi G, and Mandel LJ.** ATP depletion: a novel method to study junctional properties in epithelial tissues. I. Rearrangement of the actin cytoskeleton. *J Cell Sci* 107: 3301–3313, 1994.
2. **Ball JM, Tian P, Zeng CQ, Morris AP, and Estes MK.** Age-dependent diarrhea induced by a rotaviral nonstructural glycoprotein. *Science* 272: 101–104, 1996.
3. **Brunet JP, Cotte-Laffitte J, Linxe C, Quero AM, Geniteau-Legendre M, and Servin A.** Rotavirus infection induces an increase in intracellular calcium concentration in human intestinal epithelial cells: role in microvillar actin alteration. *J Virol* 74: 2323–2332, 2000.
4. **Canil C, Rosenshine I, Ruschkowski S, Donnenberg MS, Kaper JB, and Finlay BB.** Enteropathogenic *Escherichia coli* decreases the transepithelial electrical resistance of polarized epithelial monolayers. *Infect Immun* 61: 2755–2762, 1993.
5. **Casola A, Estes MK, Crawford SE, Ogra PL, Ernst PB, Garofalo RP, and Crowe SE.** Rotavirus infection of cultured intestinal epithelial cells induces secretion of CXC and CC chemokines. *Gastroenterology* 114: 947–955, 1998.
6. **Chambers FG, Koshy SS, Saidi RF, Clark DP, Moore RD, and Sears CL.** *Bacteroides fragilis* toxin exhibits polar activity on monolayers of human intestinal epithelial cells (T84 cells) in vitro. *Infect Immun* 65: 3561–3570, 1997.
7. **Danave IR.** Feline immunodeficiency virus decreases cell-cell communication and mitochondrial membrane potential. *J Virol* 68: 6745–6750, 1994.
8. **Dickman KG and Mandel LJ.** Differential effects of respiratory inhibitors on glycolysis in proximal tubules. *Am J Physiol Renal Fluid Electrolyte Physiol* 258: F1608–F1615, 1990.
9. **Dong Y, Zeng CQ, Ball JM, Estes MK, and Morris AP.** The rotavirus enterotoxin NSP4 mobilizes intracellular calcium in human intestinal cells by stimulating phospholipase C-mediated inositol 1,4,5-trisphosphate production. *Proc Natl Acad Sci USA* 94: 3960–3965, 1997.
10. **Fanning AS, Jameson BJ, Jesaitis LA, and Anderson JM.** The tight junction protein ZO-1 establishes a link between the transmembrane protein occludin and the actin cytoskeleton. *J Biol Chem* 273: 29745–29753, 1998.
11. **Fasano A, Uzzau S, Fiore C, and Margaretten K.** The enterotoxic effect of zonula occludens toxin on rabbit small intestine involves the paracellular pathway. *Gastroenterology* 112: 839–846, 1997.
12. **Finlay BB and Falkow S.** Salmonella interactions with polarized human intestinal Caco-2 epithelial cells. *J Infect Dis* 162: 1096–1106, 1990.
13. **Garry RF.** Sindbisvirus infection increases hexose transport in quiescent cells. *Virology* 155: 378–391, 1986.
14. **Hidalgo IJ, Raub TJ, and Borchardt RT.** Characterization of the human colon carcinoma cell line (Caco-2) as a model system for intestinal epithelial permeability. *Gastroenterology* 96: 736–749, 1989.
15. **Isolauri E, Juntunen M, Wiren S, Vuorinen P, and Koivula T.** Intestinal permeability changes in acute gastroenteritis: effects of clinical factors and nutritional management. *J Pediatr Gastroenterol Nutr* 8: 466–473, 1989.
16. **Jalonen T, Isolauri E, Heyman M, Crain-Denoyelle AM, Sillanaukee P, and Koivula T.** Increased β-lactoglobulin absorption during rotavirus enteritis in infants: relationship to sugar permeability. *Pediatr Res* 30: 290–293, 1991.
17. **Jourdan N, Brunet JP, Sapin C, Blais A, Cotte-Laffitte J, Forestier F, Quero AM, Trugnan G, and Servin AL.** Rotavirus infection reduces sucrase-isomaltase expression in human intestinal epithelial cells by perturbing protein targeting and organization of microvillar cytoskeleton. *J Virol* 72: 7228–7236, 1998.
18. **Jourdan N, Maurice M, Delautier D, Quero AM, Servin AL, and Trugnan G.** Rotavirus is released from the apical surface of cultured human intestinal cells through nonconventional vesicular transport that bypasses the Golgi apparatus. *J Virol* 71: 8268–8278, 1997.
19. **Kapikian AZ and Chanock RM. .** Rotaviruses. In: *Virology*, 2nd ed., edited by Fields BN, Knipe DM, Chanock RM, Hirsch MS, Joseph LM, Monath TP, and Roizman B. New York: Raven, 1990, p. 1353–1404.
20. **Kennedy M, Denenberg AG, Szabo C, and Salzman AL.** Poly(ADP-ribose) synthetase activation mediates increased permeability induced by peroxynitrite in Caco-2BBe cells. *Gastroenterology* 114: 510–518, 1998.
21. **Kirkwood CD, Bishop RF, and Coulson BS.** Attachment and growth of human rotaviruses RV-3 and S12/85 in Caco-2 cells depend on VP4. *J Virol* 72: 9348–9352, 1998.
22. **Landidni MP.** Early enhanced glucose uptake in human cytomegalovirus-infected cells. *J Virol* 65: 1229–1332, 1984.
23. **Lewis JA.** Inhibition of mitochondrial function by interferon. *J Biol Chem* 271: 13184–13190, 1996.
24. **Lopez-Vancell R, Beaty G, Stefani E, Rodriguez-Boulan EE, and Cereijido M.** Changes in paracellular and cellular ionic permeabilities of monolayers of MDCK cells infected with influenza or vesicular stomatitis viruses. *J Membr Biol* 81: 171–180, 1984.
25. **Madara JL and Stafford J.** Interferon-γ directly affects barrier function of cultured intestinal epithelial monolayers. *J Clin Invest* 83: 724–727, 1989.
26. **Madsen KL, Yanchar NL, Sigalet DL, Reigel T, and Fedorak RN.** FK506 increases permeability in rat intestine by inhibiting mitochondrial function. *Gastroenterology* 109: 107–114, 1995.
27. **Marano CW, Lewis SA, Garulacan LA, Soler AP, and Mullin JM.** Tumor necrosis factor-α increases sodium and chloride conductance across the tight junction of Caco-2BBe, a human intestinal epithelial cell line. *J Membr Biol* 161: 263–274, 1998.
28. **McKay DM, Benjamin MA, and Lu J.** CD4(+) T cells mediate superantigen-induced abnormalities in murine jejunal ion transport. *Am J Physiol Gastrointest Liver Physiol* 275: G29–G38, 1998.
29. **Menconi MJ, Salzman AL, Unno N, Ezzell RM, Casey DM, Brown DA, Tsuji Y, and Fink MP.** Acidosis induces hyperpermeability in Caco-2BBe cultured intestinal epithelial monolayers. *Am J Physiol Gastrointest Liver Physiol* 272: G1007–G1021, 1997.
30. **Molitoris BA, Dahl R, and Hosford M.** Cellular ATP depletion induces disruption of the spectrin cytoskeletal network. *Am J Physiol Renal Fluid Electrolyte Physiol* 271: F790–F798, 1996.
31. **Obiso RJ Jr, Azghani AO, and Wilkins TD.** The bacteroides fragilis toxin fragilysin disrupts the paracellular barrier of epithelial cells. *Infect Immun* 65: 1431–1439, 1997.
32. **Offit PA, Clark HF, Kornstein MJ, and Plotkin SA.** A murine model for oral infection with a primate rotavirus (simian SA11). *J Virol* 51: 233–236, 1984.
33. **Panja A, Goldberg S, Eckmann L, Krishen P, and Mayer L.** The regulation and functional consequence of proinflammatory cytokine binding on human intestinal epithelial cells. *J Immunol* 161: 3675–3684, 1998.
34. **Pasternak CA.** Regulation of glucose uptake by stressed cells. *J Cell Physiol* 149: 324–331, 1991.
35. **Pasternak CA.** Stress-induced increase of hexose transport as a novel index of cytopathic effects in virus-infected cells. *Virology* 166: 379–386, 1988.
36. **Philpott DJ, McKay DM, Mak W, Perdue MH, and Sherman PM.** Signal transduction pathways involved in enterohemorrhagic *Escherichia coli*-induced alterations in T84 epithelial permeability. *Infect Immun* 66: 1680–1687, 1998.
37. **Rojo G.** Migration of mitochondria to viral assembly sites in African swine fever virus-infected cells. *J Virol* 72: 7583–7588, 1998.
38. **Salzman AL, Menconi MJ, Unno N, Ezzell RM, Casey DM, Gonzalez PK, and Fink MP.** Nitric oxide dilates tight junctions and depletes ATP in cultured Caco- 2BBe intestinal epithelial monolayers. *Am J Physiol Gastrointest Liver Physiol* 268: G361–G373, 1995.
39. **Sheth R, Anderson J, Sato T, Oh B, Hempson SJ, Rollo E, Mackow ER, and Shaw RD.** Rotavirus stimulates IL-8 secretion from cultured epithelial cells. *Virology* 221: 251–259, 1996.

40. **Spitz J, Yuhan R, Koutsouris A, Blatt C, Alverdy J, and Hecht G.** Enteropathogenic *Escherichia coli* adherence to intestinal epithelial monolayers diminishes barrier function. *Am J Physiol Gastrointest Liver Physiol* 268: G374–G379, 1995.
41. **Stockmann M, Fromm M, Schmitz H, Schmidt W, Riecken EO, and Schulzke JD.** Duodenal biopsies of HIV-infected patients with diarrhoea exhibit epithelial barrier defects but no active secretion. *AIDS* 12: 43–51, 1998.
42. **Svensson L, Finlay BB, Bass D, von Bonsdorff CH, and Greenberg HB.** Symmetric infection of rotavirus on polarized human intestinal epithelial (Caco-2) cells. *J Virol* 65: 4190–4197, 1991.
43. **Sviderskaya EV.** Cellular stress causes accumulation of the glucose transporter at the surface of cells independently of their insulin sensitivity. *J Membr Biol* 149: 133–140, 1996.
44. **Taylor CT, Dzus AL, and Colgan SP.** Autocrine regulation of epithelial permeability by hypoxia: role for polarized release of tumor necrosis factor alpha. *Gastroenterology* 114: 657–668, 1998.
45. **Tian P, Hu Y, Schilling WP, Lindsay DA, Eiden J, and Estes MK.** The nonstructural glycoprotein of rotavirus affects intracellular calcium levels. *J Virol* 68: 251–257, 1994.
46. **Tripuraneni J, Koutsouris A, Pestic L, De Lanerolle P, and Hecht G.** The toxin of diarrheic shellfish poisoning, okadaic acid, increases intestinal epithelial paracellular permeability. *Gastroenterology* 112: 100–108, 1997.
47. **Tsukamoto T and Nigam SK.** Role of tyrosine phosphorylation in the reassembly of occludin and other tight junction proteins. *Am J Physiol Renal Physiol* 276: F737–F750, 1999.
48. **Tsukamoto T and Nigam SK.** Tight junction proteins form large complexes and associate with the cytoskeleton in an ATP depletion model for reversible junction assembly. *J Biol Chem* 272: 16133–16139, 1997.
49. **Tsukita S, Furuse M, and Itoh M.** Structual and signalling molecules come together at tight junctions. *Curr Opin Cell Biol* 11: 628–633, 1999.
50. **Uhnoo IS, Freihorst J, Riepenhoff-Talty M, Fisher JE, and Ogra PL.** Effect of rotavirus infection and malnutrition on uptake of a dietary antigen in the intestine. *Pediatr Res* 27: 153–160, 1990.
51. **Unno N, Baba S, and Fink MP.** Cytosolic ionized Ca^{2+} modulates chemical hypoxia-induced hyperpermeability in intestinal epithelial monolayers. *Am J Physiol Gastrointest Liver Physiol* 274: G700–G708, 1998.
52. **Unno N, Menconi MJ, Salzman AL, Smith M, Hagen S, Ge Y, Ezzell RM, and Fink MP.** Hyperpermeability and ATP depletion induced by chronic hypoxia or glycolytic inhibition in Caco-2BBe monolayers. *Am J Physiol Gastrointest Liver Physiol* 270: G1010–G1021, 1996.
53. **Yuhan R, Koutsouris A, Savkovic SD, and Hecht G.** Enteropathogenic *Escherichia coli*-induced myosin light chain phosphorylation alters intestinal epithelial permeability. *Gastroenterology* 113: 1873–1882, 1997.